ARTICLE IN PRESS

Journal of Non-Crystalline Solids xxx (xxxx) xxx



Contents lists available at ScienceDirect

Journal of Non-Crystalline Solids

journal homepage: www.elsevier.com/locate/jnoncrysol



Enhancement of ZnSe stability during optical composite processing via atomic layer deposition

Matthieu Chazot ^{a,*}, Alexandros Kostogiannes ^a, Matthew Julian ^a, Corbin Feit ^b, Jaynlynn Sosa ^b, Myungkoo Kang ^a, Cesar Blanco ^a, Justin Cook ^a, Vincent Rodriguez ^c, Frederic Adamietz ^c, Dominique Verreault ^c, Parag Banerjee ^{b,d,e,f}, Kenneth Schepler ^a, Martin C. Richardson ^a, Kathleen A. Richardson ^{a,b}

- ^a CREOL, College of Optics and Photonics, University of Central Florida, Orlando, FL 32816, USA
- ^b Department of Materials Science and Engineering, University of Central Florida, Orlando, FL 32816, USA
- c Institut des Sciences Moléculaires, Université de Bordeaux, CNRS UMR 5255, 351 cours de la libération, Talence Cedex 33405, France
- ^d Renewable Energy and Chemical Transformations (REACT) Cluster, University of Central Florida, Orlando, FL 32816, USA
- ^e Nano Science and Technology Center, University of Central Florida, Orlando, FL 32816, USA
- ^f Florida Solar Energy Center, University of Central Florida, Orlando, FL 32816, USA

ABSTRACT

This study evaluates the impact and stability behavior of a candidate protective shell of Al_2O_3 which aims to hinder the dissolution of ZnSe in As-S-Se glass systems during the so-called 'grinding-remelt' process. Atomic Layer Deposition (ALD) was chosen as the route to conformal shell coating and the role of resulting film attributes on powder and bulk composite properties were assessed to ascertain how ALD film attributes aided stability in the chalcogenide glass melt environment. It is shown that an ozone pre-treatment, performed on the ZnSe powders prior to the ALD, improves particle stability, resulting in a significant decrease of the dissolution behavior of coated powders. This enhanced stability increases with shell thickness and with the use of ozone pretreatment step on the powders. Coating chemistry and structure evaluated via XPS and HR-TEM illustrates the mechanism of dissolution for different ZnSe coated particles at varying loading levels in the glass matrix.

1. Introduction

Since the demonstration of the first laser by Maiman in 1960 [1], research in laser science has continued to push the limits of laser performance in terms of power, frequency, bandwidth or pulse duration. Such advances were always defined by the attributes of the host optical material. Laser-based systems have found applications in many fields such as telecommunication, medicine, welding, cutting, writing and spectroscopy but solid state sources with form-factors suitable for use in some key mid-infrared (MIR) spectral ranges remain a challenge. The current absence of existing MIR high-power fiber laser systems emitting across the 3-5 µm spectral region that aligns with the atmospheric transmission window [2] has fueled extensive investigations into new doped crystalline and glass hosts [3]. The need in the MIR has been motivated by the growing interest in a range of civilian and defense applications related to remote sensing of chemicals, medical imaging and diagnostics, and infrared (IR) countermeasures against heat-seeking missiles [4]. To fulfill the requirements of a suitable laser capable of emitting in the 3–5 μ m spectral window in a form insensitive to misalignment, one of the approaches explored over the past few years is the production of composite materials made of ZnSe micro/nano-crystals doped with ferrous ions (Fe²⁺) that are embedded in an IR transparent chalcogenide glass (ChG) matrix [5–12]. A glass matrix host with a suitably engineered crystallization stability which is amenable to large loading levels of dopant crystals which could be fiberized, offers numerous advantages towards the above applications.

Among all transition metals (TM) ions that can be integrated in the ZnSe lattice, Fe^{2+} has been shown as viable for lasing in the 3–5 μm range. This is due to the tetrahedral coordination of the TM dopant ion [13–15] and its dopant/crystal field environment that provides a broad absorption and emission band due to the strong electron-phonon coupling between the lattice and the active ion [13,16]. Such a local environment cannot readily be obtained in a glass host due to its disordered network environments.

Efforts to disperse Fe^{2+} :ZnSe micro/nano-crystals into a glass host have been carried out by multiple teams with the goal of producing an

E-mail address: matthieuanthonyalexandre.chazot@ucf.edu (M. Chazot).

https://doi.org/10.1016/j.jnoncrysol.2021.121259

Received 3 August 2021; Received in revised form 24 October 2021; Accepted 25 October 2021 0022-3093/© 2021 Elsevier B.V. All rights reserved.

^{*} Corresponding author.

active fiber media that could meet the needs of a robust monolithic laser system that is stable against misalignment, and compatible with any cooling system that is required to maintain a good control of the beam quality for high power loading. While the ability of ChGs to be drawn into fiber is a well-known fact [5,17-19], this is difficult for crystalline media, though recent efforts have shown promise via integration directly into the core of optical fibers during the drawing process [20]. Another synthesis route toward the production of candidate hosts for MIR fiber lasers is the direct production of Fe^{2+} doped ZnSe crystalline media into the core of a silica capillary by high pressure chemical vapor deposition (HPCVD) [21]. While suitable spectroscopic attributes have been shown, the presence of a hole in the center of the optical fiber represents a critical limitation of poor optical gain in the final fiber laser active media. Recently, promising results to fill the hole has been shown by using chemical vapor transport [22].

To obtain a homogeneous composite material with a well-dispersed secondary crystalline phase (micro or nano-particles) in the glass matrix. two main approaches can be used. The first relies on the formation of a glass followed by its partial crystallization during a post-synthesis heat treatment step [11]. This route, while possible, requires tailoring the composition of the glass matrix in order to specifically favor the nucleation and growth of ZnSe nanocrystals, at the expense of any other; this strategy is difficult due to the ability to control selective crystal growth in IR transparent glasses. The second is based on a two-step synthesis protocol that consists of grinding a glass and then mixing it with the desired ZnSe micro/nano-crystals powders prior to remelt [5]. This technique will be referred to as the "grinding remelt" technique. Target material attributes for such an approach demand good physical stability of the crystalline dopant within the melt chemistry at temperatures and times associated with the remelt process. Additionally, no phase transformation must occur, the dopant species must not diffuse out of the crystal, and refractive index matching between the crystallite and the host matrix must be maintained after the remelt and subsequent fiberization. Lastly, doped crystallite and glass matrix stability (against dissolution and further crystallization of new phases or crystallite growth) must be maintained during fiber formation. These attributes define the complexity of the multi-material processing challenge.

To realize a homogeneous composite material comprised of well dispersed, dissolution-resistant particles in a ChG host that exhibits low optical loss (absorption and scatter), no crystallization of undesired phases, a matrix that preserve the attributes of the active Fe²⁺:ZnSe crystalline phase and is amenable to being drawn into a fiber without a subsequent increase in loss, the choice has been made to use the grinding remelt technique in this study. Our choice relies on the method's advantage in allowing unique control of the dopant and matrix glass particle properties, prior to and during their incorporation in the composite material. The present study expands on how one might carry out such optimization in these various attributes in a repeatable manner to enable a high quality preform suitable for making low loss fiber.

In a previous publication [5], we presented a study on the development of an optimized glass composition designated as base glass (BG); this base glass, containing As-S and Se has been designed as the composite's matrix, tuned to match the refractive index of ZnSe. The optical and viscosity properties as well as the very good fiber drawing capability of this glass, of composition 94.6 As₂S₃ – 5.4 As₂Se₃, was demonstrated. In the second part of this publication, we investigated the stability and dissolution behavior of (bare) ZnSe in this BG host as a function of the time and the temperature of the remelt heat treatment. The results revealed a propensity of ZnSe to be dissolved during the melting process and the formation of ZnS micro-crystals that increased when rising the time and temperature of remelt. These results illustrated the challenge of maintaining the stability of Fe:ZnSe particles when mixed into a ChG glass matrix and how such stability is essential to maintain the characteristic absorption and emission behavior required for lasing in the target spectral regime.

The objective of the present study is to show a method that stabilizes

to eliminate the dissolution behavior of ZnSe in the base glass (BG) matrix during the remelt process. Here we investigate the use of a core/ shell crystallite design where the ZnSe shell chemistry and morphology attributes have been engineered to ensure survivability during the composite material synthesis. The material selected to form the shell is Al₂O₃ due to its stability at BG (re)melt temperatures and it's diffusion barrier characteristics [23]. These attributes enhance the likelihood of preventing ZnSe decomposition and reprecipitation with the sulfur present in the glass matrix (resulting in ZnS), along with any iron diffusion out of ZnSe micro-crystals. Additionally, the very high melting temperature and thermodynamic stability of Al2O3 enhance the likelihood that any partial degradation of the alumina shell would be small in the context of the low melt temperatures ($\sim\!650\,^{\circ}\text{C}$) and short melt times (hrs) of the remelt process. The preparation of core/shell particles employing Al₂O₃ as a protective layer via atomic layer deposition (ALD) [24–26] has been extensively studied in other applications. Indeed, the self-limiting nature of ALD leads to the formation of smooth, conformal, continuous and pin-hole free Al₂O₃ films [24], desirable attributes to prevent the dissolution of ZnSe core particles. It is envisioned that promising ALD coating strategies shown to stabilize ZnSe particles can be directly extended to active Fe:ZnSe crystallites.

In this work, we present results on the use, for the first time to our knowledge, of ZnSe/Al₂O₃ - core/shell particles made by ALD in an optical composite. We report on the dissolution behavior of microparticles during the remelt process in a ChG matrix, the effect of the shell thickness, the loading level and an ozone pre-treatment of powders on the stability of the coated particles. These variables are studied by examining composites with X-ray diffraction (XRD) and Raman spectroscopy. On the other hand, the use of ozone, instead of the commonly used H2O, as an active oxidant during the ALD process can be employed to improve the quality of resulting ALD Al₂O₃ films [27,28]; this quality is improved since the formation of defects such as Al-Al and OH bonds and carbon contamination from the precursor trimethylaluminum, is reduced. Here, we will show how ozone treatment can favorably impact the stability of ZnSe coated particles as a pre-treatment step, before the ALD process. We will also present the impact of the loading level on the IR transmission behavior of the composite materials. In a second part of our study, the effect of the ozone treatment on the powders prior to ALD will be examined by XPS, and finally the quality of the shell will be investigated using transmission electron microscopy (TEM).

2. Experimental section

2.1. Preparation of core-shell ZnSe particles

Commercial bare ZnSe powders (0.5 g batch), with a size of 10 µm and less, was placed into a 'barrel reactor' and loaded into an ALD viscous flow reactor for treatment. This is shown in Fig. 1. Details of this system have been reported previously from the perspective of depositing films on planar substrates [29]. Here the ALD reactor is suitably modified to accommodate powder samples. The rotating barrel reactor (1.5" in diameter and 2" long) is made of 316 steel and is lined with Teflon®. The magnetic drive assembly (Transfer Engineering and Manufacturing Inc.,) rotates the barrel along its cylindrical axis at 24 RPM to enable tumbling of the ZnSe powders and enable coating of all particle surfaces. The barrel has openings in the center on both ends to allow gasses to pass through, while preventing powder loss. Alternate pulses of trimethylaluminum (TMA) (0.5 s) and deionized (DI) $\mathrm{H}_2\mathrm{O}$ (1 s) separated with Ar purge (75 sccm) for 20 s were used. The temperature of the TMA and DI H₂O were maintained at room temperature and the furnace temperature was set at 180 $^{\circ}$ C. The ALD chamber pressure was < 1 Torr throughout the deposition.

2.2. Glass and composite material synthesis

The melt quenching technique was used to prepare ChGs of

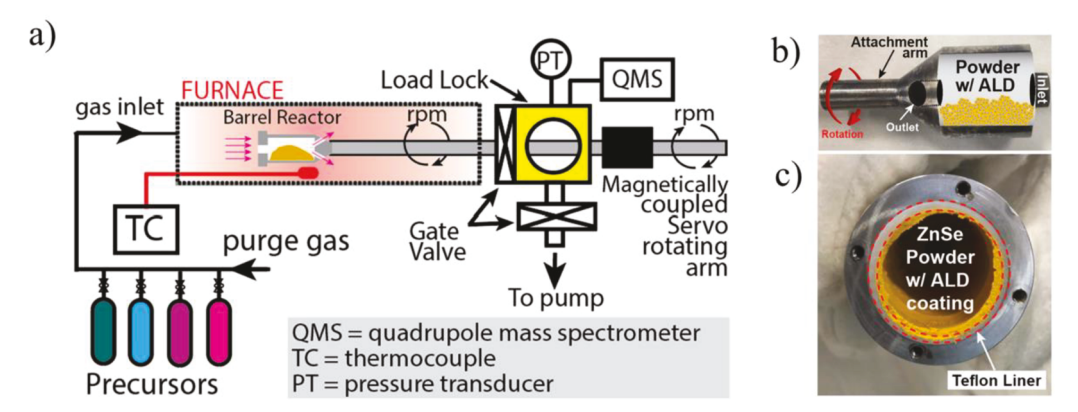


Fig. 1. (a) Schematic of the ALD viscous flow furnace reactor showing barrel reactor inserted inside the furnace. (b) Cut-out figure of the barrel reactor showing the inlet / outlet and attachment arm. (c) Front view of the opened barrel reactor with the ZnSe powder coated with ALD Al_2O_3 .

composition 94.6 As₂S₃ - 5.4 As₂Se₃, starting from high purity (5 N) elements: sulfur (S), selenium (Se) and arsenic (As) (from Alfa-Aesar), that were stored in a glovebox under controlled atmosphere (H₂O < 1 ppm and $O_2 < 0.1$ ppm) prior to glass fabrication. The raw materials were introduced in a silica ampoule, which was then sealed under primary vacuum (10^{-2} Torr) with a hydrogen/oxygen torch. Batch materials were subsequently placed in a rocking furnace and heated at a rate of 1 $^{\circ}$ C/min up to 750 $^{\circ}$ C, for a dwell time of 14 h. After dwell, the glasses were air-quenched at 600 °C and annealed at 190 °C for 4 h. All ChGs prepared from the same lot of elemental starting materials were ground using a planetary ball mill with tungsten carbide (WC) jar and balls in ambient lab conditions. Powders were then sieved using a sieve shaker (DuraTap™ Sieve Shaker, Advantech) with decreasing sieve grid sizes of 125, 53, and 25 μ m. Resultant micro-particles with sizes of 25 μ m or less were used to prepare composite material. ChG powders were sieved inside a MBraun glovebox to reduce the exposure time of powders to the ambient lab environment and minimize moisture adsorption. This handling protocol [30] is critical to minimize moisture-related impurities, due to the overlap of the mid-IR absorption bands of OH- and chalcogen-hydride species with the target Fe:ZnSe emission band. Batches of 4 g of ground ChG and crystalline ZnSe coated powders were mixed manually in the glovebox and then introduced in a new silica ampoule. The powders were then baked for removal of adsorbed water under primary vacuum (10^{-2} Torr) at a temperature of 150 °C for 1 h. After sealing under primary vacuum, the mixture was placed in a rocking furnace and heated at a rate of 1.8 °C/min up to the final melting temperature of 650°C for different dwell times (1, 2, 4 and 8 h). This temperature was selected for its corresponding ChG viscosity which is low enough to enable good homogenization of the particles in the melt and the release of any bubbles which can form due to agitation, while being high enough to avoid the sedimentation of particles prior to quenching. At the end of the synthesis time, the furnace was placed in a vertical position, the melt was pulled out and quenched directly using forced air. Subsequently, the composite materials were annealed at 190 °C for 4 h.

2.3. Materials characterization

Fourier transform infrared (FTIR) transmission data were recorded using a ThermoFisher Nicolet Is5 FTIR spectrometer with a spectral resolution of 4 cm⁻¹ and 32 accumulations. Parent glass and composite samples containing glass and crystal powder were both evaluated. ZnSe powder particle size was determined by optical microscopy combined with second harmonic generation (SHG) spectroscopy on a custom-built scanning SHG microscope [31]. In the SHG system, the excitation source was a 1064 nm picosecond laser (Leukos Opera), which delivers 50 ps pulses at a repetition rate of 1 MHz. The incident laser light was set at an average power of 10 mW and focused into the sample with a near-IR

 $20\times$ objective (Mitutoyo M-PLAN APO, NA 0.4). The resultant SHG at 532 nm was collected in the backward direction using a photomultiplier tube. The ZnSe micro-crystal size was extracted by measuring the size of particles with ImageJ software [32] on two images, confirming the vendor specification with particles size of 10 μm and less. In order to avoid particle aggregation that could lead to false particle sizing, ZnSe particles were dispersed on a microscope slide after ultrasonic processing to reduce agglomeration and stirring in an alcohol (ethanol) solution. The image analysis of the dried residue was made after complete evaporation of the solvent.

X-ray diffraction (XRD) data of the parent glass and composite-containing crystallites were collected at room temperature, using a PANalytical Empyrean XRD instrument with a beam power of 1.8 kW, a beam wavelength of $\lambda_{\text{Cu},K\alpha}=0.15418$ nm, and a beam current of 40 mA at room temperature. The XRD patterns of possible crystalline species were identified using Highscore software and the Joint Committee on Powder Diffraction Standards (JCPDS) PDF files of ZnS blende (No. 005-0566) and ZnSe blende (No. 037-1463). XRD data have been normalized over the intensity value of the most intense peak.

Any changes to the ZnSe particle surface chemistry were probed by X-ray photoelectron spectroscopy (XPS) using an ESCALAB-250Xi XPS system. Experiments were performed at a pressure below 7×10^{-9} mbar using Al-K α monochromatic radiation and an operating power of 300 W (15 kV, 20 mA). XPS data analysis and peak deconvolutions were carried out using XPS Peak 41 software. Binding energies were calibrated using the C 1 s peak at 284.5 eV.

Samples for transmission electron microscopy (TEM) were prepared by suspending the powders in alcohol via ultrasonication and depositing a drop of the suspension on a copper grid covered with a carbon film. The grid was air-dried for 15 min. High-resolution TEM (HRTEM) and Scanning TEM coupled with energy dispersive X-Ray spectroscopy (STEM-EDX) experiments were performed on a JEOL 2200 FS equipped with a field emission gun operating at 200 kV with a point-to-point resolution of 0.23 nm. High-resolution micrographs were acquired with a Gatan Ultrascan CCD 2kx2k camera and digital diffractograms were calculated with the Gatan Digital Micrograph software. Moreover, in order to be representative and statistically meaningful, multiple images from several regions of various samples were recorded and the most characteristic results are presented here.

3. Results and discussion

3.1. Composite materials

Fig. 2 shows the normalized XRD data of composite materials made of ZnSe coated particles incorporated in a base glass matrix of composition $94.6~As_2S_3 - 5.4~As_2Se_3$ using the grinding remelt process and prepared under different conditions. The experimental XRD data of ZnS,

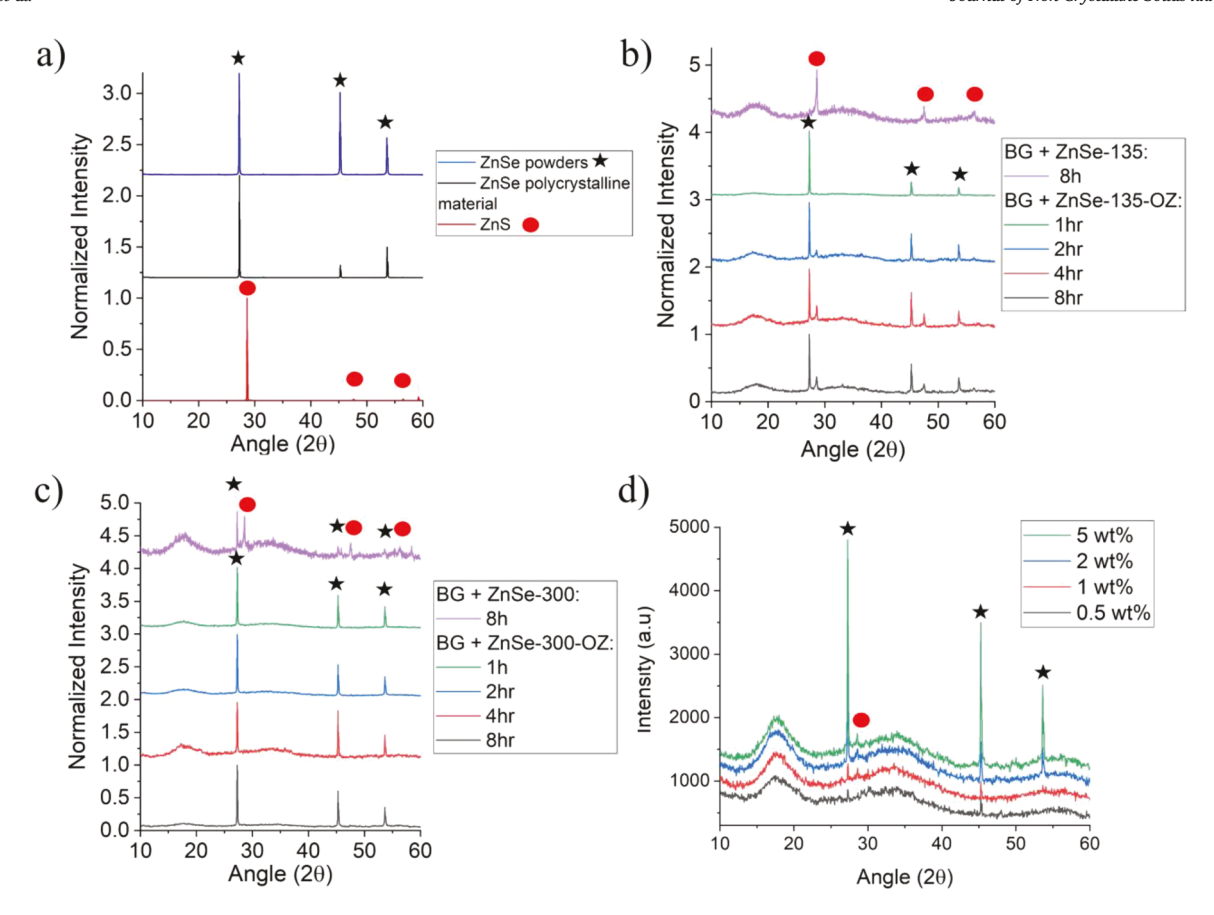


Fig. 2. Normalized XRD data of (a) ZnSe and ZnS reference crystals and powders, (b) composite materials prepared with ZnSe-135 and 135-OZ coated powders, (c) ZnSe-300 and 300-OZ coated powders as a function of remelt time duration, and d) XRD patterns for composite materials prepared with different loading levels of ZnSe-300-OZ and a remelt time of 4 h. The diffractograms have been vertically shifted to allow improved clarity.

ZnSe crystals and ZnSe powders, prepared by grinding a part of the same ZnSe crystal, are displayed in Fig. 2.a as a reference. It is interesting to note that the relative intensities of the (111) peak at 27.20°, (220) peak at 45.23° and (311) peak at 53.15° monotonically change in a descending order for the ZnSe powders, which is consistent with the literature [33,34], whereas the opposite is observed for the (220) and (311) peaks of our ZnSe polycrystalline coupon. This is because the ZnSe coupon used in this paper is indeed a textured polycrystalline material, which can be due to the sample fabrication method [35]. Grinding this coupon into powders as for effect of retains the randomness in terms of texture and loose the textural directionality. Fig. 2.b and c present the diffractograms of the composite materials made of ZnSe powders, coated with varying numbers of ALD cycles (135 versus 300 cycles) in order to study the impact of number of deposition cycles on resulting shell thickness. The resulting thickness variation (greater cycles resulted in a thicker shell) was then used to assess particle dissolution behavior of the powders, following identical remelting protocols. Assuming a 0.1 nm deposition rate / cycle [36,37], the powders prepared with 135 and 300 cycles are estimated to have shell thicknesses of 13 and 30 nm, respectively. The impact of different ALD deposition protocols (with and without ozone pretreatment of ZnSe powders) and remelt duration (1, 2, 4 and 8 h) are also illustrated in Fig. 2.b and c. All composite materials were prepared under the same remelt temperature (650 °C) and loading level (10 wt% of ZnSe coated powders). In examining Fig. 2.b the diffraction pattern of the composite made from ZnSe-135 cycle coated powders (without ozone treatment) reveals only the presence of ZnS, identified with the PDF files of ZnS blende (No. 005-0566). This observation of ZnS crystallization is a sign of a complete dissolution of ZnSe micro-particles and reprecipitation of Zn with S in the glass melt. Indeed, our previous work [5] under similar conditions showed the complete dissolution of bare (uncoated) ZnSe in As-S-Se glasses, followed by the formation of ZnS micro-crystals. This suggests that the 135 cycle layer without any pre-treatment is not robust enough to survive the melt conditions. On the other hand, the composite materials made of ZnSe-135-OZ coated powders, which are particles that underwent an ozone (OZ) pretreatment, show minor dissolution of ZnSe based on the observation of a relatively small ZnS peak as compared to that of initial ZnSe species which is still evident in the composite. This result highlights how the ozone pretreatment applied to the ZnSe powders before the ALD step increases significantly the stability of the coated powders during the remelt process. In comparison, the XRD data of composites made of ZnSe-300-OZ coated powders (Fig. 2.c), particles expected to have a 2 to 3 times larger shell thickness as compared to that of their ZnSe-135-OZ counterparts, shows only ZnSe diffraction peaks (patterns corresponding to JCPDS data files of ZnSe Blende No. 037-1463) following remelt, suggesting that this film thickness is sufficient to completely prevent particle dissolution. Once again, we compare this finding to patterns from the composite made of ZnSe-300 powders (without an ozone pretreatment) which exhibits peaks corresponding to ZnSe but also some ZnS. This comparison reveals that once again the ozone pretreatment significantly improves the stability of the particles. Further, the increase in the shell thickness (higher numbers of ALD cycles) plays a role on the stability of the powders. It is interesting to note from Fig. 2.b that the relative intensity of the ZnS peak does not necessarily increase linearly with the time of remelt (especially between 4 and 8 h) for the composite made of ZnSe-135-OZ powders. This suggests that any decomposition/recrystallization is likely limited by available Zn which is fully decomposed during the initial few hours of melting.

Fig 2.d presents the XRD diffraction patters of composites made of

ZnSe-300-OZ powders with different loading levels and prepared using the same melt condition: 650 °C and 4 h of remelt. This figure shows that the intensities of ZnSe peaks rise with the increase in the loading level of ZnSe coated powders. However, despite the use of ZnSe-300-OZ powders in all cases, one can see the presence of a small peak at around 28.5 that corresponds to ZnS. Hence, this suggests that while our ALD protocol is largely repeatable, some variation in shell thickness and or integrity, may be occurring. The difference between the composites made for the loading level series and the ones that comprise the series with different heat treatment times (Fig. 2.c) is the batches of coated powders used that were prepared on different days. Even if the ZnSe-300-OZ powders that were used for those two different series were prepared following the same protocol, it appears that there may be some

variation in shell attributes from one batch to another. This variation may be related to minor variations in humidity; while powders are stored in a glove box, ALD treatment carried out in ambient lab conditions during the winter in Florida (FL, USA), likely have much lower levels that those prepared in the spring and summer. It is important to highlight that despite this slight 'leakage' leading to low levels of ZnS, the peaks corresponding to ZnSe are strongly dominating, enlightening the protective behavior of the shell during remelt as compared to that of our previous work where no shell was present [5]. Hereafter, the two series displayed on Fig 2.c and d will be referred as the "remelt duration" series and the "loading level" series respectively.

In order to further confirm the presence of ZnSe coated particles as well as their survivability during the remelt process, Raman

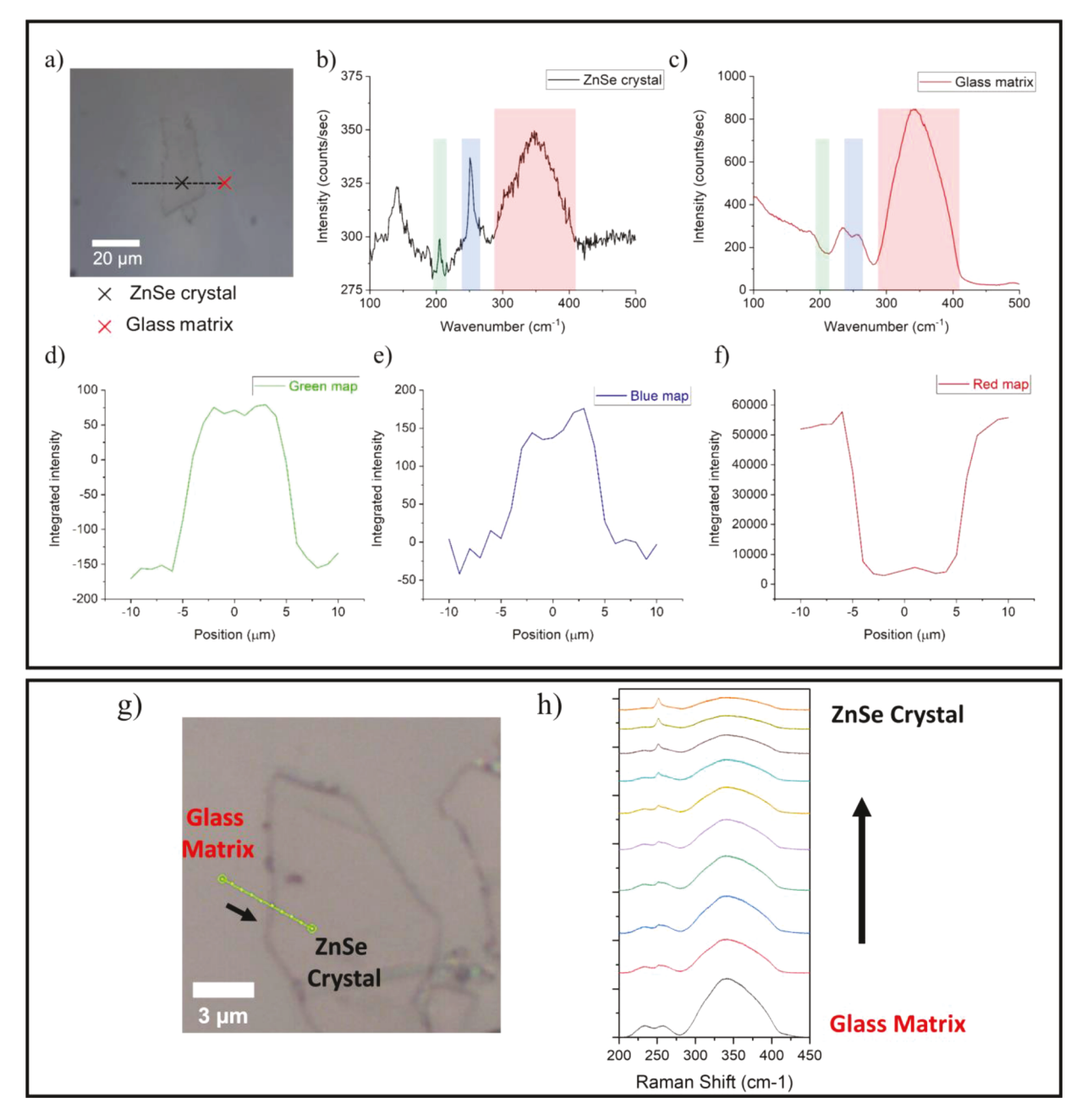


Fig. 3. Top - (a) Optical micrograph of a crystal showing the Raman line scan performed on a composite material made with 0.5wt% 300-OZ ZnSe-coated powders, with the Raman spectra of (b) the center of the crystal (black cross) and (c) the outer zone of the crystal (red cross), followed by the integrated intensity of the Raman peaks in (d) green, (e) blue and (f) red. Bottom – (g) Optical micrograph of a second crystal showing the Raman line scan and h) the corresponding Raman spectra performed on a composite material made with 0.5 wt% 300-OZ ZnSe-coated powders. (For interpretation of the references to color in this figure legend, the reader is referred to the web version of this article).

spectroscopy was used to characterize the surface of a composite material made with 0.5wt% of ZnSe-300-OZ particles. Fig. 3 illustrates two Raman line scans (top and bottom) performed on the composite. Fig. 3.a presents the optical image of the first zone characterized with the presence of a particle on the surface. Fig. 3.b and c show the Raman spectra collected at the center and at the outer edge of the particle, respectively. The Raman peaks corresponding to the 2TA, TO and LO modes of ZnSe [38], respectively at 150, 205 and 250 cm⁻¹, can be clearly observed in the spectra of Fig. 3.b. These modes are completely absent out of the crystal zone (Fig. 3.c), where the Raman spectra exhibits peaks characteristic of an As-S-Se chalcogenide glass matrix with broad Raman peaks at around 235, 260 and 340 cm⁻¹. The bands at 235 and 260 cm⁻¹ can be assigned to As-Se vibration in AsCh₃ units, while the band at and 340 $\text{cm}^{-1}\,\bar{\text{i}}\text{s}$ generally ascribed to As–S vibration in AsS $_3$ pyramidal units [39]. Fig. 3.d-f present the integrated intensity of the green, blue and red regions depicted in Fig. 3.b and c corresponding to the TO and LO modes of ZnSe (green and blue regions), and the main As-S vibrational mode characteristic of an As-S glass (red region). The integrated intensity of Fig. 3.d and e show an increase in the region that corresponds optically to the crystal zone, whereas the opposite is observed in Fig. 3.f with a dip in the integrated intensity of the peak corresponding to the main glass elementary units. From this analysis it is clear that this entity observed on the surface of the composite is a ZnSe crystal. This, in addition to the XRD analysis, confirms the presence of ZnSe micro-crystals in the composite materials made of ZnSe-300-OZ powders. This was further validated via Raman analysis using a Horiba LabRAM HR Evolution Nano set up. Here, a different zone of the same composite (Fig 3.g and h) was analyzed using a 785 nm excitation at 50 mW and a magnification of 100X. A small peak corresponding to the LO mode of ZnSe at around 250 cm⁻¹ begins to appear as the line scan passes the interface from the base glass to the middle of the ZnSe microcrystal. This has also been confirmed on other composites (not presented here) made from the same coated particles. Despite the observation of crystalline entities with no characteristic Raman peaks corresponding to ZnSe or ZnS, this methodology could not resolve any presence of ZnS micro-crystals in composite materials made of ZnSe-135-OZ nor on samples from the loading level series made of ZnSe-300-OZ powders. While it could be possible that these species might correspond to ZnS, Raman bands were not observed using laser excitation intensities up to the threshold where damage in the glass-composite surface was observed. This could also be due in part to the low Raman response of ZnS as compared to that of the parent glass matrix. Thus, the Raman spectra of the composite is dominated by the vibrational modes of the glass, despite the use of a confocal Raman microscope with optimized conditions to reduce the Rayleigh length of the laser beam and the confocal volume analyzed.

Fig. 4 presents the FTIR absorbance spectra of the loading level composite materials series (from 0.5 to 5 wt%) with the spectra for the parent base glass included as a reference. The FTIR spectra of the composites show a transmission window that corresponds to that of the original As-S-Se BG with a multiphonon cutoff around 12 µm. It is important to mention that ZnSe crystal (not presented here) does not present any spectral features in that region. The spectra also show an increase of the absorption in the short wavelength region as a function of the loading level, though all samples containing ZnSe show an enhanced As-O band in the longwave around 10.5 μm, most likely realized during powder handling c.a As-containing BG grinding process, prior to remelt. This shortwave evolution is typical of a Mie scattering absorption tail, where the magnitude of loss increases with the decrease in wavelength. The evolution suggests the presence of aggregates and / or micron size entities having a slight different refractive index than that of the glass matrix, despite the efforts made to ensure index matching with the BG matrix. One cannot exclude the possibility of a slight deviation of the glass stoichiometry as well as some partial oxidation of the crystallite and/or the BG particles after the different powder handling steps of the composite preparation, leading to such scatter loss due to induce index

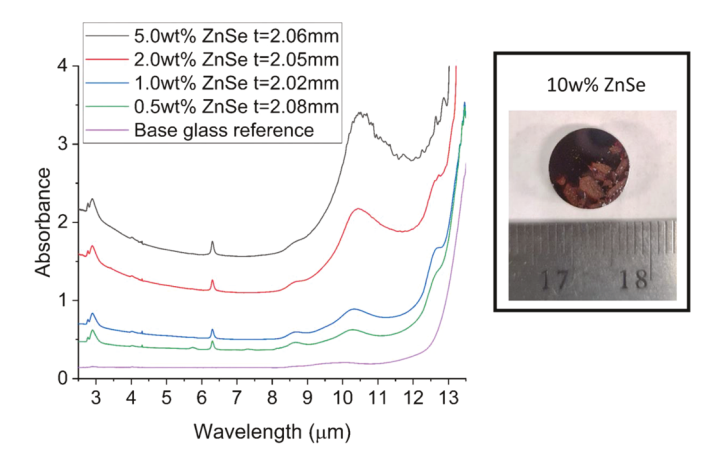


Fig. 4. (left) Absorbance in the IR of composite materials made of ZnSe-300-OZ ZnSe-coated powders in function of loading levels. The thickness "t" is also reported for each sample for comparison. (Right) Photograph of a composite material with 10 wt% of ZnSe-300-OZ ZnSe-coated powders illustrating powder agglomeration during remelt.

mismatch along with any notable agglomeration that might occur in the melt. This scales with number of particles, hence the loss tail is more extensive for the composite with a higher loading level. The observation of minor ZnS diffraction peaks for the composite materials that compose this series (Fig. 2d) and the presence of large aggregates visible by eye in materials with the highest loading levels (5wt% and more), such as seen in the material presented in Fig. 4 (right) having a loading level of 10wt %, leads us to think that the two hypotheses *c.a* impact of aggregates and the presence of ZnS particles, are responsible for the Mie scattering losses observed here.

One can clearly see other features in the FTIR spectra. Specifically, one can note the presence of several extrinsic absorption features that can be related to impurities in the form of hydrides, hydroxides and oxides compounds. The main observable absorption peaks correspond to vibrational modes of: -S-H at 4 μ m; -O-H $^-$ at 2.92 μ m; -Se-H at 4.12 μ m; H_2O at 6.3 $\mu m;$ -As-O at 8.9 μm and 9.5 $\mu m;$ and finally -Se-O at 10.1 μm [19]. Despite the use of high purity raw elements (stored in a glove box under controlled environment) to prepare the base glass matrices, the presence of these extrinsic absorptions and their corresponding impurities can be created and retained in the grinding step, following the glass preparation, as grinding is carried out in an un-purged ball mill jar (WC) in ambient air. That, in addition to the fact that these elements did not undergo any additional purification (distillation of sulfur or selenium, and sublimation of arsenic), explains the observation of large extrinsic absorption in the IR for these composite materials. This is further confirmed by the appearance and increase of absorption bands related to water and hydrides in the composites as compared to that of the reference base glass (before grinding and remelt).

3.2. ZnSe coated powders characterization

In an attempt to understand and explain the impact that the Ozone (UV-O₃) treatment has on the stability of coated powders during the remelt process, a hydrophilic study and a XPS analysis has been performed on untreated (as received) and UV-O₃ treated ZnSe powders. In Fig. 5.a the water suspension behavior after 5 min of (i) untreated, and (ii) UV-O₃ treated ZnSe powders are demonstrated. The untreated ZnSe powder remains largely afloat, whereas, the UV-O₃ treated powder sinks to the bottom of the glass vial. This illustrates the role of the UV-O₃ treatment on the powders which improves the hydrophilicity of their surfaces, enhancing their wettability and dispersion in water. This result indicates that surface oxidation of ZnSe might be the reason explaining the enhanced stability behavior against dissolution of the ZnSe coated particles when exposed to an ozone pretreatment, by enabling a better

M. Chazot et al.

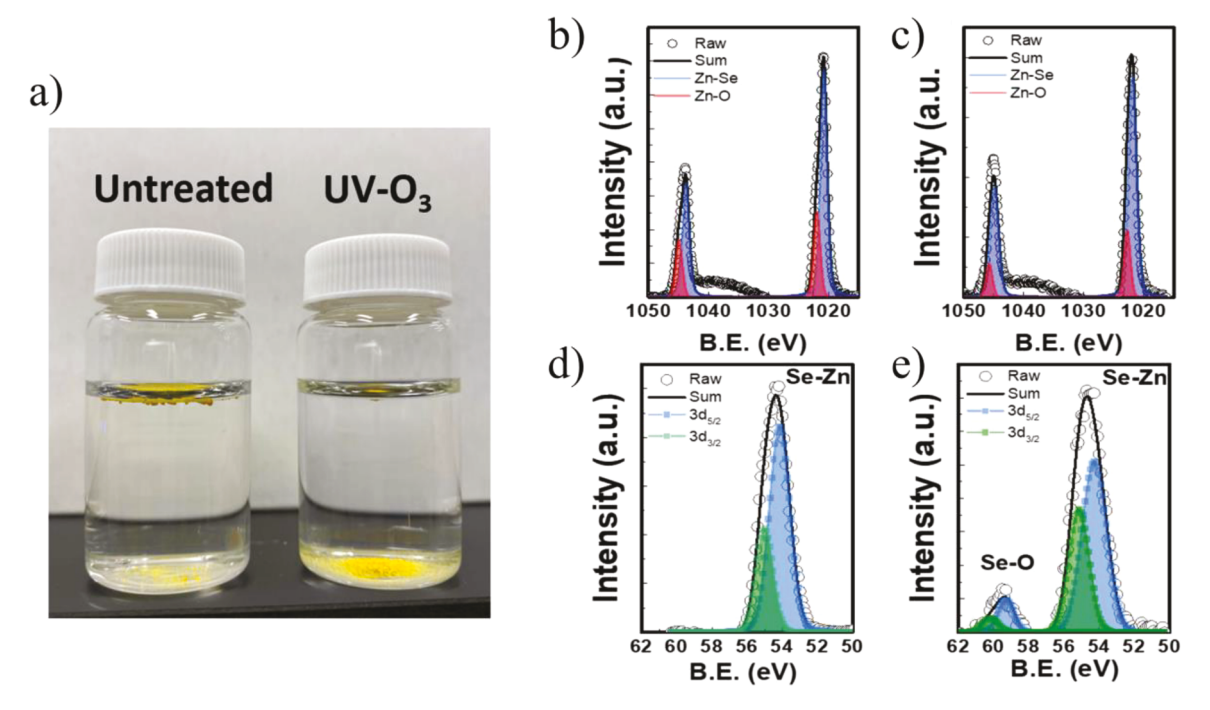


Fig. 5. (a) Image of untreated (commercial) ZnSe particles that remain suspended in DI (left) water while treatment with UV-O₃ (right) causes the particles to sink to the bottom. (b) XPS fine spectrum of Zn 2p from the untreated, as-received ZnSe showing primarily Zn-Se bonding with a small amount of Zn-O bonding. (c) XPS fine spectrum of Zn 2p from the UV-O₃ treated ZnSe showing primarily Zn-Se bonding with a small amount of Zn-O bonding, similar to the untreated ZnSe sample. (d) XPS fine spectrum of Se 3d from untreated, as-received ZnSe showing Se-Zn bonding. (e) XPS fine spectrum of Se 3d from the UV-O₃ treated ZnSe showing Se-Zn bonding but importantly, Se-O formation as well.

deposition of ALD Al₂O₃ coating.

In order to confirm the oxidation state of the ZnSe surface after ozone pretreatment, the ZnSe powders were probed by x-ray photoelectron spectroscopy (XPS). The Zn 2p spectra of the as-received Zn-Se is shown in Fig. 5.b. The spectrum can be deconvoluted into two peaks. The Zn 2p_{3/2} peak at 1020.8 eV corresponds to the Zn-Se bonding, whereas the peak at 1021.8 eV corresponds to Zn-O [40,41]. It is interesting to note that even with ZnO detected via XPS, the bulk surface properties of ZnSe remain hydrophobic. When the surface of the ZnSe powder is pretreated with UV-O₃ (Fig. 5.c), the $2p_{3/2}$ peak shifts to higher binding energy (B. E.) - 1021.9 eV for Zn-Se and 1022.6 eV for Zn-O. This shift can be attributed to increased ZnO or ZnOH at the interface after UV-O3 treatment [41]. The effect is even more pronounced for the Se fine spectra. The as-received ZnSe powder (Fig. 5.d) shows peaks at 54.15 eV and 55.01 eV corresponding to Se $3d_{5/2}$ and Se $3d_{3/2}$, respectively. These peaks are related to the Se-Zn bond. We note that the peaks are closely separated with a spin-orbit splitting of 0.86 eV only [42]. After UV-O₃ pretreatment, the B.E. of the Se $3d_{5/2}$ are shifted slightly higher to 54.28 eV and that of $3d_{3/2}$ to 55.14 eV (Fig. 5.e). More interestingly, additional peaks are observed at 59.3 eV (3d $_{5/2}$) and 60.16 eV (3d $_{3/2}$) corresponding to the Se-O bond formation [40,41,43]. The oxidation of the ZnSe is considered to cleave the Zn-Se bonding to form SeO₂ [44]. It is possible that elemental Se may exist at the surface, but the B.E. is convoluted with SeO₂ and Se(OH)₄ species [41]. Nevertheless, the XPS analysis reveals that pretreating ZnSe with UV-O₃ generates oxides of Zn and Se. Specifically, while ZnO is already present on the surface of untreated ZnSe, presence of SeO2 is clearly observed upon UV-O3 pretreatment. The surface preconditioning is certainly critical for the subsequent growth of ALD Al₂O₃ and probably results in lower incubation cycles as compared to that seen on the bare, untreated ZnSe surface. This could explain the higher resilience against dissolution of the ozone treated powders, through the formation of thicker shells of better quality.

To ascertain shell coating conformality and overall layer quality and thickness uniformity (both within a single particle and across particles

form the same deposition run), STEM-EDX chemical mapping and HR-TEM images of ZnSe particles coated by ALD with different cycle numbers c.a 135 and 300 cycles and on different batches was performed. Fig. 6.a and b show the TEM image and the chemical mapping of ZnSe-300-OZ particles coming from the batch used to prepare the remelt duration series presented in Fig 2.c. These powders all underwent 300 ALD cycles after an ozone pre-treatment. One can distinguish from the contrast on the TEM image, a lighter layer all around the particles. This layer overlaps perfectly with the violet region on the chemical mapping in Fig. 6.b which correspond to Al + O elements. In comparison, the core of the particle overlaps the green areas that correspond to Zn + Se elements. This elemental mapping clearly reveals the presence of an Al₂O₃ shell around the ZnSe particles. Meanwhile, one can observe in Fig. 6.b some zones where the shell seems to be discontinuous (red arrow). However, as can be seen on the contrast STEM image (red arrow on Fig. 6.a) a uniform shell is seen around the whole particle, with the shell exhibiting excellent conformal coating as intended for the material deposited by ALD. The lack of Al + O signal in certain zones can possibly be due to a shadowing effect of emitted X-ray by thick particles and to the relative position of the EDX detector. On the other hand, Fig. 6.c and d show the TEM image and the chemical mapping of particles coming from the batch of ZnSe-300-OZ powders used for the loading level series (Fig. 2.d). Even if the majority of the particles observed were covered with a shell, it was possible to find some micro-particles that illustrate a complete lack of protective layer around them, as the one observed in Fig. 6.c and d. This is something that has not been observed in the first batch discussed previously (deposited in the early winter); we postulate this variation in shell integrity may be the reason for the small dissolution observed in the loading level series where small amounts of ZnS formed. Even if it is hard to draw any conclusion based on a microscopic analysis, it is important to mention that such a presence of uncoated particles seemed to be statistically more significant in ZnSe powder undergoing ALD coating without an ozone pretreatment (not shown here). In the meantime, Fig. 6.e presents a STEM image of another ZnSe-300-OZ particle coming from the duration remelt batch, where it can be

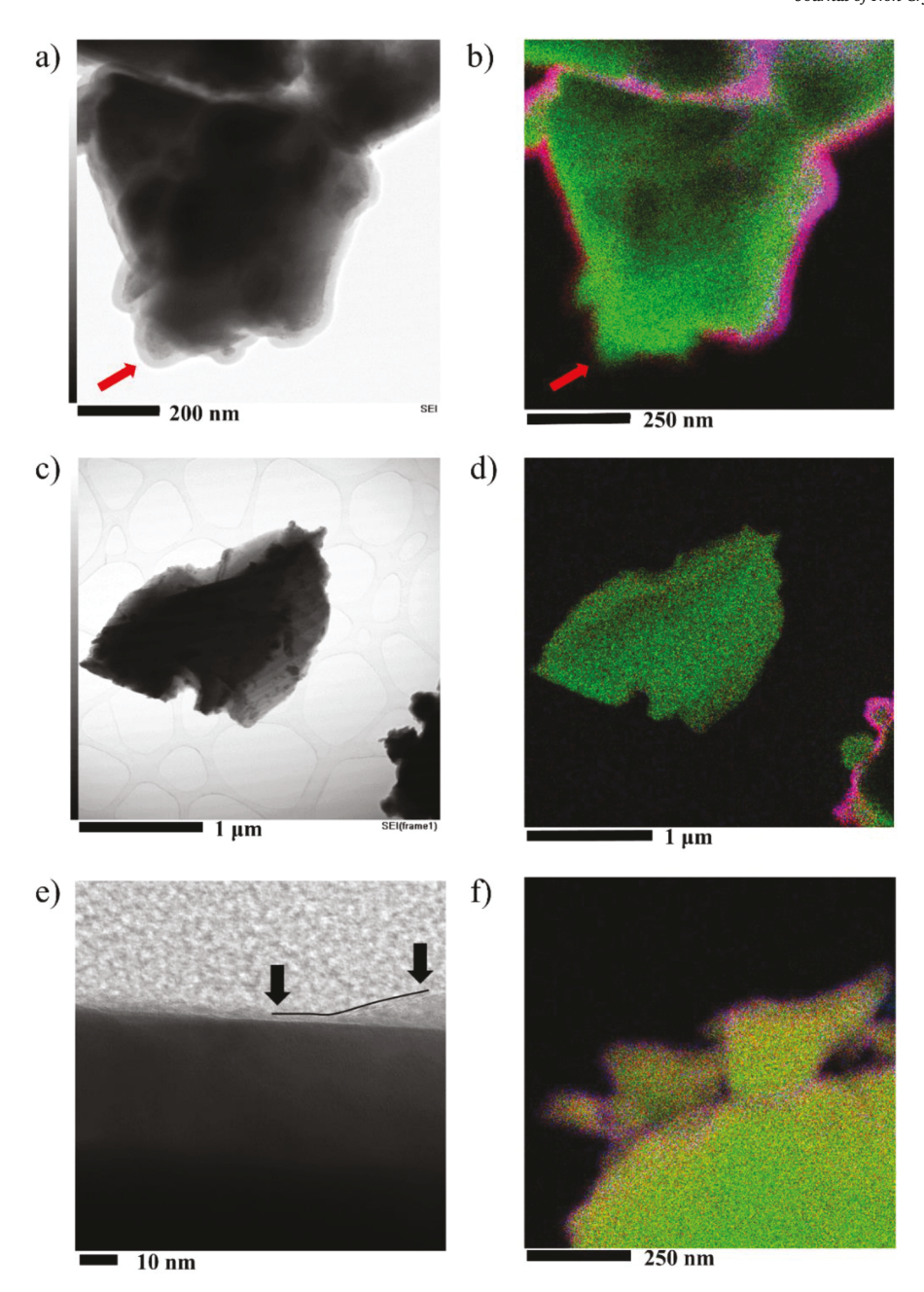


Fig. 6. (a), (b), (c), (d) and (e) TEM and STEM-EDX mapping images of ZnSe-300-OZ powders; and (f) STEM-EDX mapping images of ZnSe-135-OZ powders.

seen that the shell is not perfectly homogeneous in terms of its thickness and shows, in some areas, regions where the alumina layer is thinner than expected. Fig. 6.f illustrates the chemical mapping of the ZnSe-135-OZ powders. As for its ZnSe-300-OZ counterparts, the shell seems to be conformal, although because it is much thinner it is hard to clearly assess shell thickness uniformity. The shell thicknesses of the particles have been measured on over 30 images of each sample. The thickness has been found to be between 5 and 10 nm for the ZnSe-135-OZ and 28-35 nm for the ZnSe-300-OZ coated powders, which is expected, given that a rate of deposition of 0.1 nm / cycle is reported in the literature [36]' [37]. Meanwhile, the shell measured around the ZnSe-135-OZ powders is very thin as compared to that of ZnSe-300-OZ, and it is possible that the layer may be altered or that some aggregates observed in TEM may have broken during the powder handling (mixing of BG + coated powders). This could also lead to ZnSe dissolution leading to the presence of ZnS peaks when using ZnSe-135-OZ powders to prepare the composite materials. This, in addition to the possibility that some particles may not completely be covered, as observed for the loading level series, can explain the ZnSe dissolution and the formation of ZnS observed in the ZnSe-135-OZ series. We don't believe this disintegration of particles to be related to a shell dissolution over the time of heat treatment, since the relative intensities of ZnS peaks does not increase linearly with the time of remelt. Conversely, the absence of ZnS diffraction peaks for the composite made of ZnSe-300-OZ powders for the duration remelt series, is consistent with the absence of observable discontinuities in the shell of ZnSe-300-OZ powders revealed by TEM. One could also argue that the dissolution may be the results of a sublimation of ZnSe particles that could then induce the breakage of the shell at the temperature used for the preparation of the composite materials (650 °C). However, thermogravimetric analysis (TGA) was conducted up to 800°C (not presented here), with a ramp rate of 3 °C/min under nitrogen with a purge flow rate of 100 mL/min. This analysis did not reveal any sign of mass loss, thereby excluding this hypothesis.

Concurrent with these observations of shell thickness, one can also

M. Chazot et al.

see the presence of aggregates in Fig. 6.a, b and f. These particles have a size of few microns and are composed of sub-micron particles. These aggregates could also be responsible for the scattering losses observed on the FTIR spectra in Fig. 5, in addition to the presence of ZnS crystals. While undesirable, we believe the agglomeration of particles during the ALD process can be reduced by modifying the reactor characteristic and the large aggregates that could be formed during the ALD (- 20 μm and more) can be selectively removed by a simple sieving of the coated particles after the deposition.

5. Conclusion

As an attempt to suppress the dissolution behavior of ZnSe in a chalcogenide base glass matrix of composition 94.6 As₂S₃ – 5.4 As₂Se₃, a new protocol involving the formation of an amorphous Al₂O₃ protective shell on the particles by ALD has been proposed. The XRD pattern of the resultant composite materials made by the so-called grinding remelt technique, with different ALD cycle numbers, coated particle loading levels and remelt duration have been studied. The results reveal a drastic reduction of the extent of ZnSe particle dissolution using ozone as a pretreatment step followed by alumina coating of the ZnSe particle. A concurrent decrease in the dissolution with the increase of the shell thickness, was also observed. The presence of ZnSe micro-crystals within the doped ChG composite were confirmed by combined Raman and optical microscopy. Moreover, the effect of an ozone pretreatment performed on the powders prior to the ALD was investigated, and results show a significant increase in the survivability of the ZnSe particles as compared to their non-ozone treated counterparts, while prepared under identical remelt conditions. Further analysis on ozone treated powders by XPS shows that the treatment induces an oxidation of the surface particle and the formation of a Se-O layer, which results in a modification of powder surface chemistry rendering the particles hydrophilic. We believe this hydrophilicity greatly enhances the interface whereby the ALD coating can adhere, as it is believed to reduce the incubation cycles required to form stable layer formation during the deposition of Al₂O₃. It was also noted that some variability in the ALD process conditions still remain, as batches of coated powders prepared with identical cycle times exhibited different dissolution stability, as evidenced by the slight presence of ZnS in some composites formed with 300-OZ powders. A batch-to-batch analysis on the powders by HR-TEM revealed the formation of a conformal Al₂O₃ shell on the majority of the powders, but also the absence of the protective layer on some particles of the batch suggesting a partial dissolution when used for the preparation of the composites. Lastly, the transmission properties of the composite materials have been characterized by FTIR and Mie scattering losses were observed. These losses appeared to increase with the loading level and can be related to either the presence of ZnS micro-crystals formed as a result of partial dissolution and/or the presence of aggregates of coated ZnSe particles during the remelt process. This agglomeration was most pronounced for the highest loading levels. Lastly, the role of powder handling clearly shows the stepwise increase in extrinsic absorption species associated with the multi-step composite fabrication steps. Nevertheless, this study shows that, when complete on all particles and homogenous, (i) the ozone pretreatment of ZnSe powders before ALD, significantly enhances the stability of ZnSe coated powders and (ii) the Al₂O₃ shell made by ALD is effective against the dissolution of ZnSe during a remelt process at temperatures as high as 650 °C and for a duration of up to 8 h. We believe that these results represent a major step towards the preparation of new composite materials that would include active micro-particles in a ChG matrix, through the use of the ALD process as a way to protect the particles by the formation of a conformal shell. The next steps of this work will involve the preparation of high purity and aggregate free Fe:ZnSe/Al $_2$ O $_3$ + BG composite materials followed by their luminescence characterization on bulk and fiber forms. Purification of elements and powders as incremental steps in the process will be performed to reduce absorption in the critical $3-5 \mu m$

window. Additional work is also being conducted to better understand the impact of ozone treatment on powders and the number of incubation cycles required for the formation of Al_2O_3 by ALD. These results open the door towards the fabrication of Fe:ZnSe doped glass composite preforms which will be the subject of our next paper describing the optical performance of bulk composite as compared to doped fiber.

CRediT authorship contribution statement

Matthieu Chazot: Conceptualization, Methodology, Investigation, Validation, Writing - original draft, Visualization, Supervision. Alexandros Kostogiannes: Methodology, Investigation. Matthew Julian: Methodology, Investigation. Corbin Feit: Methodology, Investigation. Jaynlynn Sosa: Methodology, Investigation. Myungkoo Kang: Methodology, Investigation, Writing - review & editing, Supervision. Cesar Blanco: Methodology, Investigation. Justin Cook: . Vincent Rodriguez: Methodology, Investigation, Writing – review & editing. Frederic Adamietz: Methodology, Investigation. Dominique Verreault: Methodology, Investigation. Parag Banerjee: Conceptualization, Methodology, Formal analysis, Writing - review & editing. Kenneth Schepler: Conceptualization, Methodology, Formal analysis, Writing - review & editing, Project administration, Funding acquisition. Martin C. Richardson: Conceptualization, Project administration, Funding acquisition. Kathleen A. Richardson: Conceptualization, Methodology, Formal analysis, Writing - review & editing, Supervision, Project administration, Funding acquisition.

Declaration of Competing Interest

The authors declare that they have no known competing financial interests or personal relationships that could have appeared to influence the work reported in this paper.

Acknowledgment

The authors thank the financial support of AFOSR for the Grant FA9550-19-1-0127. This work was partially supported by the University of Central Florida under the preeminent Postdoctoral Program (P3). VR and DV thanks financial support from the French National Research Agency (ANR) in the framework of the "Investments for the Future" Programme IdEx Bordeaux LAPHIA (ANR-10-IDEX-03-02). The authors would like to thank Jérôme Majimel and Guillaume Salek from UGIEL Services and the platform of materials characterization: Placamat (Univ. Bordeaux, CNRS, PLACAMAT, UMS 3626, PESSAC, France), for their technical support on TEM measurements. CF and JS were partially supported by NSF award number 1908167. Authors acknowledge the NSF MRI: ECCS: 1726636 and MCF-AMPAC facility at the University of Central Florida.

References

- T.H. Maiman, Stimulated optical radiation in ruby, Nature 187 (493) (1960) 493–494.
- [2] S.D. Jackson, R.K. Jain, Fiber-based sources of coherent MIR radiation: key advances and future prospects (invited), Opt. Express 28 (21) (2020) 30964, https://doi.org/10.1364/OE.400003.
- [3] M.G.C. Jr, S.C. Aro, S.A. McDaniel, et al., Continuous wave Fe²⁺: ZnSe mid-IR optical fiber lasers, Opt. Express 28 (20) (2020) 30263–30274.
- [4] L. Isaenko, A. Yelisseyev, A. Tkachuk, et al., Crystalline laser and nonlinear optical materials for the mid-IR, in: M. Ebrahim-Zadeh, I.T. Sorokina (Eds.), Mid-Infrared Coherent Sources and Applications, Springer Science + Business Media B.V, 2008, pp. 3–168.
- [5] M. Chazot, C. Arias, M. Kang, et al., Investigation of ZnSe stability and dissolution behavior in As-S-Se chalcogenide glasses, J. Non Cryst. Solids 555 (2021), 120619, https://doi.org/10.1016/j.jnoncrysol.2020.120619 (December 2020).
- [6] D.V. Martyshkin, J.T. Goldstein, V.V. Fedorov, S.B. Mirov, Crystalline Cr2+: ZnSe/chalcogenide glass composites as active mid-IR materials, Opt. Lett. 36 (9) (2011) 1530–1532, https://doi.org/10.1364/OL.36.001530.
- [7] R.A. Mironov, E.V. Karaksina, A.O. Zabezhailov, R.M. Shaposhnikov, M. F. Churbanov, E.M. Dianov, Mid-IR luminescence of Cr2+: II–VI crystals in

- chalcogenide glass fibres, Quant. Electron. 40 (9) (2010) 828–829, https://doi.org/10.1070/QE2010v040n09ABEH014408.
- [8] E.V. Karaksina, L.A. Ketkova, M.F. Churbanov, E.M. Dianov, Preparation of mid-IR-active AS₂S₃/ZnS(ZnSe): Cr2+ composites, Inorg. Mater. 49 (3) (2013) 223–229, https://doi.org/10.1134/S0020168513030072.
- [9] A. Yang, J. Qiu, J. Ren, et al., 1.8–2.7 μm emission from As-S-Se chalcogenide glasses containing ZnSe: Cr2+ particles, J. Non Cryst. Solids 508 (2019) 21–25, https://doi.org/10.1016/j.jnoncrysol.2019.01.007. January.
- [10] E.V. Karaksina, V.S. Shiryaev, L.A. Ketkova, Preparation of composite materials for fiber optics based on chalcogenide glasses containing ZnS(ZnSe): Cr(2+) crystals, J. Non Cryst. Solids 377 (2013) 220–224, https://doi.org/10.1016/j. inoncrysol.2012.12.021.
- [11] X. Lu, J. Li, L. Yang, et al., Broadband mid-infrared (2.5–5.5µm) emission from Co2 + /Fe2+ Co-doped chalcogenide glass ceramics, Opt. Lett. 45 (9) (2020) 2676, https://doi.org/10.1364/ol.392190.
- [12] X. Lu, Z. Lai, R. Zhang, et al., Ultrabroadband mid-infrared emission from Cr2+-doped infrared transparent chalcogenide glass ceramics embedded with thermally grown ZnS nanorods, J. Eur. Ceram. Soc. 39 (11) (2019) 3373–3379, https://doi.org/10.1016/j.jeur.ceramsoc.2019.04.048.
- [13] J.W. Evans, T.R. Harris, B.R. Reddy, K.L. Schepler, P.A. Berry, Optical spectroscopy and modeling of Fe2+ ions in zinc selenide, J. Lumin. 188 (2017) 541–550, https://doi.org/10.1016/j.jlumin.2017.04.017. February.
- [14] J. Kernal, V.V. Fedorov, A. Gallian, S.B. Mirov, V.V. Badikov, 3.9–4.8µm gain-switched lasing of Fe: ZnSe at room temperature, Opt. Express 13 (26) (2005) 10608–10615, https://doi.org/10.1364/OPEX.13.010608.
- [15] V.V Fedorov, S.B. Mirov, A. Gallian, et al., 3.77-5.05-µm tunable solid-state lasers based on Fe2+-doped ZnSe crystals operating at low and room temperatures, IEEE J. Quant. Electron. 42 (9) (2006) 907–917, https://doi.org/10.1109/ JQE.2006.880119.
- [16] S. Mirov, V. Fedorov, New regimes of excitation and mid-IR lasing of transition metal doped II–VI crystals, in: M. Ebrahim-Zadeh, I.T. Sorokina (Eds.), Mid-Infrared Coherent Sources and Applications, Springer, 2008, pp. 261–314.
- [17] M. Chazot, M. El Amraoui, S. Morency, Y. Messaddeq, V. Rodriguez, Investigation of the drawing region in the production of Ge-S-I optical fibers for infrared applications, J. Non Cryst. Solids 476 (2017), https://doi.org/10.1016/j. inoncrysol.2017.09.037.
- [18] M. Chazot, M. El Amraoui, S. Morency, A. Hanafi, Y. Messaddeq, V. Rodriguez, Thermal characterizations and investigation of the drawing region in Ge-As-S glasses for IR optical fibers, J. Non Cryst. Solids (2019), https://doi.org/10.1016/j. inoncrysol.2018.12.022.
- [19] G.E. Snopatin, V.S. Shiryaev, V.G. Plotnichenko, E.M. Dianov, M.F. Churbanov, High-purity chalcogenide glasses for fiber optics, Inorg. Mater. 45 (13) (2009) 1439–1460, https://doi.org/10.1134/S0020168509130019.
- [20] J. Ballato, E. Snitzer, Fabrication of fibers with high rare-earth concentrations for Faraday isolator applications, Appl. Opt. 34 (30) (1995) 6848–6854.
- [21] J.R. Sparks, R. He, N. Healy, et al., Zinc selenide optical fibers, Adv. Mater. 23 (14) (2011) 1647–1651, https://doi.org/10.1002/adma.201003214.
- [22] A.T. Hendrickson, S.C. Aro, J.R. Sparks, et al., Post-processing ZnSe optical fibers with a micro-chemical vapor transport technique, Opt. Mater. Express 10 (12) (2020) 3125–3136
- [23] D. Bae, S. Kwon, J. Oh, W. Kyoung, H. Park, Investigation of Al₂O₃ diffusion barrier layer fabricated by atomic layer deposition for flexible Cu (In, Ga) Se₂ solar cells, Renew. Energy 55 (2013) 62–68, https://doi.org/10.1016/j.renene.2012.12.024.
- [24] George S.M. Atomic layer deposition: an overview. 2010;111–131.
- [25] Sci J.V., Coile M.W., Elam J.W. High-capacity rotary drum for atomic layer deposition onto powders and small mechanical parts in a hot-walled viscous flow reactor high-capacity rotary drum for atomic layer deposition onto powders and

- small mechanical parts in a hot-walled viscous flow reactor. 2020;052403.10.1116/6.0000274.
- [26] Sci J.V., Wollmershauser J.A., Boercker J.E., Feigelson B.N. Growth per cycle of alumina atomic layer deposition on nano- and micro-powders. 2017;021519 (November 2015). 10.1116/1.4941918.
- [27] You A., Be M.A.Y., In I. Improvement in Al2O3 dielectric behavior by using ozone as an oxidant for the atomic layer deposition technique. 2013;6739(2002). 10.1063/1.1515951.
- [28] Goldstein D.N., Mccormick J.A., George S.M. Al2O3 atomic layer deposition with trimethyl aluminum and ozone studied by in situ transmission FTIR spectroscopy and quadrupole mass spectrometry. 2008;19530–19539. 10.1021/jp804296a.
- [29] Z. Gao, F. Wu, Y. Myung, et al., Standing and sitting adlayers in atomic layer deposition of ZnO, J. Vac. Sci. Technol. A Vac. Surf. Film 34 (1) (2016) 01A143, https://doi.org/10.1116/1.4938080.
- [30] Kostogiannes A. Powder optimization study towards the production of ZnSe -doped As-S-Se composite materials. to be Publ. 2021.
- [31] Gouget G., Duttine M., Durand E., Villesuzanne A., Rodriguez V. Isolating the two room-temperature polymorphs of NaNbO3: structural features, optical band gap, and reactivity. 2019. 10.1021/acsaelm.8b00125.
- [32] C.A. Schneider, W.S. Rasband, K.W. Eliceiri, NIH Image to ImageJ: 25 years of image analysis, Nat. Methods 9 (7) (2012) 671–675, https://doi.org/10.1038/ nmeth.2089.
- [33] P. Zhou, M. Zhang, L. Wang, Q. Huang, Z. Su, L. Li, Synthesis and electrochemical performance of ZnSe electrospinning nanofibers as an anode material for lithium ion and sodium ion batteries, Front. Chem. 7 (2019) 1–10, https://doi.org/ 10.3389/fchem.2019.00569. August.
- [34] F. Qiao, R. Kang, Q. Liang, Y. Cai, J. Bian, X. Hou, Tunability in the optical and electronic properties of ZnSe microspheres via Ag and Mn doping, ACS Omega 4 (2019) 12271–12277, https://doi.org/10.1021/acsomega.9b01539.
- [35] M.T. Chowdhury, A. Zubair, H. Takeda, Optical and structural characterization of ZnSe thin film fabricated by thermal vapor deposition technique, AIMS Mater. Sci. 4 (2017) 1095–1121, https://doi.org/10.3934/matersci.2017.5.1095. September.
- [36] A.W. Ott, J.W. Klaus, J.M. Johnson, S.M. George, Al₃₀₃ thin film growth on Si (100) using binary reaction sequence chemistry, Thin Solid Films 517 (20) (1997) 5950, https://doi.org/10.1016/j.tsf.2009.01.027.
- [37] M.D. Groner, F.H. Fabreguette, J.W. Elam, S.M. George, Low-temperature Al₂O₃ atomic layer deposition, Chem. Mater. (16) (2004) 639–645.
- [38] B.K. Rai, R.S. Katiyar, K.T. Chen, A. Burger, Raman and photoluminescence studies on intrinsic and Cr-doped ZnSe single crystals, J. Appl. Phys. 83 (11) (1998) 6011–6017.
- [39] W. Li, S. Seal, C. Rivero, et al., Role of S /Se ratio in chemical bonding of As-S-Se glasses investigated by Raman, X-ray photoelectron, and extended X-ray absorption fine structure spectroscopies, J. Appl. Phys. 98 (5) (2005), https://doi.org/10.1063/1.2009815.
- [40] J.R. Shallenberger, N. Hellgren, Zinc selenide analyzed by XPS zinc selenide analyzed by XPS, Surf. Sci. Spectra 27 (014020) (2020), https://doi.org/10.1116/ 6.0000165.
- [41] N. Hellgren, M.A. Steves, J. Shallenberger, S.K.O. Boyle, E. Mellott, A.R. Noble, Applied surface science effect of etching on the oxidation of zinc selenide surfaces characterized by X-ray photoelectron spectroscopy, Appl. Surf. Sci. 528 (2020), 146604, https://doi.org/10.1016/j.apsusc.2020.146604. April.
- [42] J.F. Moulder, W.F. Stickle, P.E. Sobol, K.D. Bomben, Handbook of X-Ray Photoelectron Spectrosopy, Physical Electronics Inc., 1992.
- [43] J. Herrero, A.M. Chaparro, M.T. Gutie, Morphological and compositional study of CBD-ZnSe thin films by microscopy techniques and angle resolved XPS, Thin Solid Films 358 (2000) 22–29.
- [44] J.D. Mccullough, The crystal structure of selenium dioxide, J. Am. Chem. Soc. 59 (5) (1937) 789-794.